https://doi.org/10.1016/j.mtener.2018.10.004



# Dynamically Self-activated Catalyst for Direct Synthesis of Hydrogen Peroxide ($H_2O_2$)

*Mingzi Sun, Xinyue Liu and Bolong Huang**

Department of Applied Biology and Chemical Technology, The Hong Kong Polytechnic University, Hong Hum, Kowloon, Hong Kong SAR, China.

*Email: bhuang@polyu.edu.hk

KEYWORDS: **DSHP, Passivation, Self-activate, RuNi, DFT,**

Understanding the mechanism of the dynamic process of direct synthesis of hydrogen peroxide (DSHP) will facilitate finding the highly efficient catalyst to overcome the challenges of present research. Beyond the presently known catalysts for DSHP, we predict a self-activated and novel catalyst RuNi through density functional theory (DFT) calculations. Detailed calculations have been carried out on the dynamic adsorption processes of RuNi (111) surface regarding the binding energies and surface configurations. The over-activity of Ru atoms in cleavage of adsorbates and intermediates can be balanced by the presence of Ni atoms. Most importantly, the natural enhancement of DSHP is based on the self-activation through the formation of the passivation film on the surface, which plays an essential role in the inhabitation of undesired O-O bond dissociation and the optimization of the binding energies of $H_2O_2$ and $O_2$. Hence, we have proposed a mechanism of realizing efficient DSHP based on the dynamically self-activated RuNi catalyst, which can provide guidance and inspiration for further experiments on searching for novel catalyst candidates.

## Introduction

Hydrogen peroxide($H_2O_2$), an environmentally friendly oxidant, has been considered as an alternative to replace the traditional oxidants including chlorinated oxidizers and strong acids in many chemical synthesis and industrials processes.[1-3] However, 90% of the $H_2O_2$ in the world is produced by the anthraquinone oxidation (AO) process that confronts intense energy consumption, tedious separation procedures ,and high costs.[4] This complicated method includes four main steps: hydrogenation, oxidation, hydrogen peroxide extraction and working solution treatment, which still suffers from low mass transfer efficiency in reactors, the inevitable loss of product due to organic contamination, and heavier equipment. All these issues will decrease process sustainability, increase production and maintenance costs so that alternative method to avoid these drawbacks with high efficiency is urgently needed presently. As a one-pot process, DSHP ($H_2$ + $O_2$ → $H_2O_2$) becomes the simplest way to synthesize this oxidant that can lead to a significant reduction in the capital investment and operating costs. To achieve large-scale production, research on finding a highly efficient catalyst for DSHP has become intense in recent years.[5-9] The basic reactions of DSHP are shown as the follows:

$$\mathbf{H_2 \rightarrow H^* + H^*} \quad (1)$$

$$\mathbf{O_2 \rightarrow O - O^*} \quad (2)$$

$$\mathbf{O - O^* + H^* + H^* \rightarrow H_2O_2} \quad (3)$$

Main concerns about this method are focusing on the formation of side product $H_2O$ induced by decomposition of both $O_2$ and $H_2O_2$, which will significantly lower the selectivity and productivity as shown in **Figure 1**. The non-dissociation of O-O bond during the adsorption of oxygen molecule has been considered as the determining step for the generation of $H_2O_2$. Mavrikakis *et al.* found out that the breakage of the O-O bond in either $H_2O_2^*$ or $OOH^*$ is facile to realize and carries a

majority of rate control. After breaking the O-O bond, the following H-transfer to $O^*/OH^*$ adsorbates reaction will form $H_2O^*$consequently.[5] Such dissociation of O-O bonds on transition metal surfaces can be attributed to the electrons transfer to the oxygen p* antibonding orbitals and the hybridization between p-$O_2$ and d-metal orbitals.[10] These detrimental reactions demonstrate that a high $H_2O_2$ selectivity and productivity can only be achieved by decreasing or even inhibiting the presence of OH* intermediates through low rate O-O bond cleavage. Meanwhile, a stable reaction rate of adding hydrogen atoms to adsorbed oxygen molecules is needed as well. Hence, transition metals and related alloys as active catalysts that have become the most potential candidates.[11-14] Presently, Pd-related alloys are the mainstream in catalyst research for direct synthesis of $H_2O_2$ with the highest selectivity and productivity.[12, 15, 16] Chang *et al.* summarized that reasonable adsorption energy of oxygen as well as a positive energy barrier for dissociating oxygen molecules that make Pd the ideal catalyst.[17] Moreover, the addition of another metal can significantly affect the properties of their constituent elements in lattice parameters, electronic interactions and spatial configuration, which is appealing as catalysts. Many transition metals have been chosen to optimize the performance of Pd catalyst, and Au is the most popular one.[13, 18-20] However, as the price of Pd and Au keeps increasing and has become similar with Pt recently, the potential Pd-free catalyst has become desired as Pt-free catalysts, which is insufficient.[14, 21]

Among other transition metals, Ru has a unique electron configuration as $4d^75s^1$ that can result in a much wider range of valence states and more complicated coordinated geometries, which has made them important catalysts in many chemical reactions.[22, 23] In addition, Ru is a well-known catalyst in hydrogenation, which is similar to Pd, so we could expect that Ru should exhibit relatively close or even better performance. The Ni-related catalyst is another potential choice that shows a stronger tolerance to electrolyte dissolution and lower material cost.[24] Therefore, Ru, Ni

and RuNi alloy as the catalyst or additive metal to catalyst alloy have been widely studied in direct gasoline oxidation in fuel cells and hydrogenation.[25-28] The presence of Ni can improve the catalytic performance of the Ru monometallic catalysts in terms of both activity and selectivity to the product of interest via a synergic effect between Ru and Ni.[29] The high stability of Ni-related and Ru-Ni catalysts under different reactions have also been tested in previous research.[30-32] However, even though the beneficial effects of additive metal to catalysts are real and certain, the detailed mechanisms are still under dispute. Inspired by these previous findings, RuNi bimetallic catalyst has the potential to be a novel choice of catalyst for application in the direct synthesis of $H_2O_2$.

To screen out more possible catalysts for DSHP, utilizing the DFT calculation can accelerate the processing speed by saving time on the traditional methods including synthesis and testing a large amount of different and unknown transition metal combinations. Moreover, DFT can provide guidance for future experimental works to improve certain catalyst performances, which have been used in investigating the mechanism of DSHP on Pd-related alloys in many previous works.[5, 33, 34] Hence, in this work, we will apply DFT calculations to explore the potential of an alloy catalyst with their mechanism ahead of experiments, which can benefit further experimental tests and supply further experiences on predicting new catalysts through efficient DFT methods. In this work, we propose the mechanism of the RuNi alloy as a potential catalyst in the direct synthesis of $H_2O_2$ through DFT calculations. The adsorption behaviours of primary reactants have been calculated in detail under the pure surface condition and oxygen-covered conditions. We highlight the effect of the oxygen coverage as the main factor that that allows this surface to be successfully applied to direct oxidation of hydrogen to generate $H_2O_2$.

## Calculation Setup

### Slab Models

The periodic RuNi catalyst surface will be cleaved from the fcc crystal structure model of Ni with half of the atoms replaced by Ru atoms since the co-deposited bimetal alloy has been confirmed to show primary Ni fcc structure.[27] We apply (111) surface model to be the representative model for the catalyst simulations since this surface has been proven as the most active surface in other transition metal catalyst for direct synthesis of $H_2O_2$.[5, 35] The slab models consist a total of four layers with 144 atoms (i.e. $Ru_{72}Ni_{72}$) entirely in a repeated 3x3 supercell, in which two upper layers are allowed for total relaxation, and bottom two layers are fixed as the bulk. The vacuum distance of the unit cell has been set as 8.0 Å the same as the catalyst layers to avoid interruption between the periodic unit cell to observe the adsorption and de-adsorption behaviors on the surface.

### Calculation Setting

All the calculations for adsorption behaviors and electronic structures within density functional theory (DFT) will be carried out through CASTEP package codes.[36] The generalized gradient approximation (GGA) and PBE functional basis sets are chosen with 380 eV cut-off energy in a plane-wave basis set. [37, 38] The ultrasoft pseudopotentials will be applied to describe the ex-change correlation energy and potential. The RRKJ method is chosen for the optimization of the pseudopotentials.[39] The Broyden-Fletcher-Goldfarb-Shannon (BFGS) algorithm was applied for geometry optimization through all calculations. Reciprocal space integration was performed using Monkhost-Pack k-point grids of 2×2×2 k-points in the Brillouin zone. Different orbital projectors that Ru with (4s, 4d, 4p, 5s), Ni with (3d, 4s) states and O with (2s, 2p) atoms to represent their valence states. The spin-polarization has been included in the calculation. The transition states

were performed with the complete linear and quadratic synchronous transit QST method that is embedded in CASTEP.

The binding energies ($E_B$) are calculated based on the difference between the total energy of the adsorbed surface and the total energy of the pure phase of adsorbate and the clean surface of RuNi (111) as Equation (4).

$$E_B = E_{total}(\text{Adsorbed Surface}) - E_{total}(\text{Adsorbate}) - E_{total}(\text{Pristine Surface}) \quad (4)$$

The chemical adsorption is using the similar equation as when there is one more adsorbate on the surface. The convergence settings for all the geometry optimization will be as follows: the energy tolerance for geometry relaxations requires that total energy will not exceed $5.0 \times 10^{-5}$ eV/atom; maximum ionic Hellmann−Feynman force and maximum ionic stress will be restricted within 0.1 eV/Å and 0.2 GPa, respectively. The maximum ionic displacement should be within $5.0 \times 10^{-3}$ Å.

## Results and Discussion

### Adsorption Behaviors

The dissociation speed of hydrogen molecules will happen quickly on catalyst surfaces, which has been proven by former reports on Pd-related catalysts.[40, 41] As shown in Eq. (1), the adsorption of $H_2$ will determine the generation speed of $H_2O_2$ via providing flexible hydrogen atoms near the surface, which has been investigated and summarized in **Table 1**. The binding energies of $H_2$ on the surface are very similar such that it shows no strong preference on the adsorption sites. Ni top sites are slightly more favorable for adsorption as shown in **Figure 2**. The geometry relaxation reveals that the strong interaction between the surface and $H_2$ will result in the dissociation of hydrogen molecules, in which the dissociated H atoms will be stabilized near the bridge top after

relaxation with 2.498 Å between H atoms. In contrast, the adsorption of single H atom displays even slightly higher binding energies than $H_2$, which represents that the H atoms would prefer to dissociate near the surface instead of being firmly fixed by chemical bonds with the surface. Moreover, the continuous adsorption of $H_2$ and the concentration of H atoms on the surface will not be influenced by the adsorption competition. The chemical adsorption energies of $H_2$ are not too negative that can prevent the over-binding situation to ensure the further reaction with adsorbed oxygen molecules. Such results have laid a solid foundation for next step reaction.

Conventionally, the adsorption of $O_2$ is believed to be the critical factor that influences the selectivity to $H_2O_2$ (**Equation (5)**). As the previously proposed mechanism stated[42], the breakage of O-O bonds has led to the result that the single O atom adsorbs one dissociative H* to form intermediate OH* and side product $H_2O$ as **Equation (6)-(7)**.

$$O - O \rightarrow O^* + O^* \quad (5)$$

$$O^* + H^* \rightarrow OH^* \quad (6)$$

$$OH^* + H^* \rightarrow H_2O^* \quad (7)$$

Hence, the low cleavage rate of $O_2$ is critical for achieving high selectivity and productivity of $H_2O_2$. As listed in **Table 2**, $O_2$ adsorption shows distinct selectivity for the active site on the surface, in which the threefold coordinated hollow site surrounded by three metal atoms is the most preferable and stable adsorption site. Compared with binding energies of $H_2$ listed in **Table 1**, $O_2$ shows much lower binding energies than that of $H_2$ with the catalyst surface, implying a much stronger physicochemical trend to react. This also means that at the first stage of adsorption on the pure catalyst surface, $O_2$ has more advantage than $H_2$ when competing on adsorption with

the surface. Geometry relaxation displays visible O-O bond cleavage on the hollow site with an O-O distance of 4.324 Å as **Figure 2**. This adsorption behaviour is similar to oxygen adsorption on the pure Ru surface.[43] On all the active sites of RuNi (111), $O_2$ will undergo quick dissociation and become very stable at the hollow site as the oxygen coverage. Converse to the hydrogen atom, the oxygen atom displays strong potential in forming chemical bonding on the surface due to the sharp decrease in chemical adsorption energies compared with their binding energies. This result suggests that after molecule dissociation, oxygen atoms will be strongly bonded on the hollow site of RuNi (111) surface forming an oxidation-like state, which is in agreement with that RuNi nanoparticle will easily form atmospheric oxides.[27] Similar results attained from XPS results on Ru-related catalysts also proved the existence of Ru(IV).[44]

From **Figure 3a**, we can see that even after being covered with oxygen atoms on the surface, the total density of states (TDOS) display a very similar pattern without a noticeable difference. Hence, we use the projected density of states (PDOS) of the adsorbed oxygen atoms with neighbouring metal atoms that are influenced by the adsorption behaviour to unravel the actual orbital interaction between adsorbate and the surface. It is noted that the overlapping of orbitals occurs between O-2p orbitals and d orbitals of surface metals, suggesting very active electron transfer. This modified electron density is similar with the work of Laasonen *et al.* of $O_2$ adsorption on the Pd (111) surface.[45] To support that Ru is more active in the interaction with oxygen atoms, **Figure 3b** shows a more detailed PDOS of surface metal. Between 5~7 eV below Fermi level, the O-2p orbital and Ru-4d orbital significantly overlap with each other, implying a strong interaction. Similar overlap is also found near 1~2 eV above the Fermi level. Yang *et al.* demonstrated that the overlapping between the orbitals of transition metals and O-$p_\sigma$ orbitals would facilitate the ion transfer.[46] However, such orbital overlaps can be rarely found between O atoms and Ni atoms,

which is also a crucial contributor to the total d orbital DOS. The surface configuration in **Figure 2** clearly illustrated that Ru atoms are more unstable on the surface and causes distortion induced by the surface adsorbates. It is worth considering that the transfer of electron density between the molecule and the surface will be profoundly affected by the surface configurations. [47, 48] The overlapping between Ni-3*d* and Ru-4*d* implies a weakening binding of Ni-O and Ni-H. Overall, these results all demonstrate that Ru plays as the main active sites to transfer electrons and form strong binding with adsorbates. Ni atoms can balance the catalyst activity and maintain the surface structure due to their excellent stability and high tolerance in different environments.

The stability and desorption on the surface of $H_2O_2$ are of great importance in determining the final productivity of $H_2O_2$. The dissociation of $H_2O_2$ should be largely suppressed meanwhile the binding effect of surface should not be too strong to hinder the releasing of formed $H_2O_2$ from the surface. On the pristine RuNi (111) surface, the decomposition of $H_2O_2$ will happen on all active sites, accompanying strong interaction between Ru and O on the surface that results in the cleavage of the O-O bond. As shown in Table 3, all the binding energies of $H_2O_2$ at different positions are close with the binding energies of $H_2$, in which the bridge top shows the lowest binding energy as shown in **Figure 2**. The initial state is at bridge top and the OH* intermediates have been bonded to Ru and hollow sites after geometry relaxation. The distance between oxygen atoms increases from 1.485 Å to 3.341 Å. The generation of intermediate OH* is the origin of the $H_2O$ generation.[17, 49] To achieve higher $H_2O_2$ generation efficiency, such O-O bond dissociation should be suppressed so as to prevent the formation of detrimental intermediate O* and OH*. As the main side product to influence the efficiency of DSHP, we also compare the formation of $H_2O$ and $H_2O_2$ to explore their relationship on the surface. In the left part of **Figure 4a**, the formation of $H_2O_2$ and $H_2O$ has been revealed based on the energy comparison between the adsorption of the adsorbed

species H* and O* and product molecules $H_2O_2$ and $H_2O$ at the four adsorption sites (Pd, Cu, bridge, hollow). Due to the lower adsorption energies of both products than the adsorption energies of the component species, formation of both $H_2O_2$ and $H_2O$ are energetically favorable. Notably, the $H_2O_2$ shows overall lower energies than $H_2O$, implying that the formation competition between $H_2O_2$ and $H_2O$ might lead to the lower efficiency of DSHP. For the chemisorption energies summarized in the right part of **Figure 4a**, the energies of O adsorption can be primarily downshifted when more O atoms participate. In comparison with other species as H, $H_2$ and $H_2O$, the chemisorption of $O_2$ and O atoms is relatively favorable with higher stability on the surface, which can lay the foundation of later high coverage of passivation layer on the surface.

Further investigation of the binding energies associated with adsorbate positions is discussed in **Figure 4b**, in which Ru atoms on the surface exhibit the predominant role in reacting with oxygen atoms rather than Ni. Notably, we find out that when oxygen molecule is vertical above Ru top site, oxygen molecule will become parallel above Ru under the strong interaction from Ru atom. After relaxation, Ru atom will rise from the surface and form stable bonds with the oxygen molecule. Such observations are in accordance with the electronic structure calculations in **Figure 3b**. The nanoparticle RuNi model (**Figure 4c)** has also been proven that exhibits the similar high activity of dissociating the O-O bonds in both Ru and Ni sites. To interpret the mechanism between microscopic behaviors and macroscopic experimental observations in a more detailed and reasonable method, we will carry out the investigation of the effect of such oxidation states on enhancing the catalyst performance. To summarize the possibility of such a pristine surface, we define the typical reactions towards $H_2O_2$ including the possibilities of intermediate $H_2O$ related reactions (R1-R6) as follows:

$$\begin{cases}(H_2 + O_2)_{far} \rightarrow (H_2 + O_2)_{close} \\ (H_2 + O_2)_{close} \rightarrow H_2O_2\end{cases} \quad \text{(R1)}$$

$$\begin{cases}2H_2 + 2O_2 \rightarrow 2H_2O + O_2 \\ 2H_2 + O_2 \rightarrow 2H_2O + 2O \\ 2H_2O + 2O \rightarrow 2H_2O_2\end{cases} \quad \text{(R2)}$$

$$\begin{cases}2H_2O + O_2 \rightarrow 2OH + 2H + O_2 \\ 2OH + 2H + O_2 \rightarrow 2OH + 2H + 2O \\ 2OH + 2H + 2O \rightarrow 2OOH + 2H \\ 2OOH + 2H \rightarrow 2H_2O_2\end{cases} \quad \text{(R3)}$$

$$\begin{cases}H_2 + O_2 \rightarrow 2H + 2O \\ 2H + 2O \rightarrow H_2O_2\end{cases} \quad \text{(R4)}$$

$$\begin{cases}2H_2O + O_2 \rightarrow 2H_2O + 2O \\ 2H_2O + 2O \rightarrow 2H_2O_2\end{cases} \quad \text{(R5)}$$

$$\begin{cases}H_2 + O_2 \rightarrow 2H + 2O \\ 2H + 2O \rightarrow H_2O + O \\ H_2O + O \rightarrow H_2O_2\end{cases} \quad \text{(R6)}$$

With above-considering reactions, the energetic preferences and competitions for (a) adsorptions of $H_2$ and $O_2$ as well as the bonds scissions, and (b) intermediate $H_2O$ participated reactions are the two keys guiding the direct synthesis of $H_2O_2$ on the supported catalytic system (nanoalloys). The corresponding energy diagrams in terms of chemisorption energy (ΔG) are shown in **Figure 5** Throughout R1 to R6, we found that pristine RuNi (111) surface (without oxidation passivation) exhibit high barriers in all the $H_2O_2$ synthesis reactions. Moreover, since the surface is overactive, the formation of $H_2O_2$ cannot be stabilized on the surface, accompanied by a quick and energy favorable decomposition with an evident energy drop as the arrows show. R1 reaction shows the much stronger adsorption behaviors on $H_2$ and $O_2$ as the distance between adsorbates and surface is getting smaller. R2 and R6 all utilize the formation of water as an intermediate, which require

an extremely high energy cost that represents the low possibility of oxidation of water. R4 and R5 show similar energy trend, which both experience the unstable formation of $H_2O_2$ that lead to the energy downhill to the decomposition of $H_2O_2$. However, for the reaction R3 that is initiated from $H_2O$ and $O_2$ with active intermediates like OH or OOH, and ended at $H_2O_2$, the energy displays a downhill trend but with an exceptionally high energy cost for water adsorption on the surface. In addition, the final step to form $H_2O_2$ also confronts another barrier. Therefore, all these reactions confirm the difficulties of DSHP directly happening on pristine RuNi (111) surface without any treatment of the surface. To realize the DSHP on such RuNi (111) surface, we believe the further adsorption behaviours will be largely influenced by the surface adsorbates passivation coverage, which will be oxygen atoms according to our preliminary results. In other reports, partial oxidation on Pd or Pt catalysts for DSHP have been proposed to be responsible for the high catalyst activity.[2, 42] In addition, XPS results have proved that transition metals will experience different valance states on the surface.[50] During the synthesis of transition metal catalyst, pre-treatments like high-temperature heating treatment seems to have exhibited important effects but the mechanism has never been clarified.[20] Hence, we will discuss the influence from such oxygen passivation coverage and the corresponding effect to the DSHP.

**Self-activation with the Passivation film**

Previous calculations have shown that the hollow site is most energy favorable for mono oxygen atom after relaxation, so the oxygen passivation layer will be expected to initially form on the hollow sites of the surface. To specify the actual effect induced by such passivation layer, we applied two oxygen atoms at the hollow site and related binding with intermediate adsorbates on top to observe the adsorption process as the start. Based on the hexagonal surface configuration, three different oxygen position arrangements including ortho-, meta- and para-position (**Figure**

**6a**) are presented to study the adsorption behaviours of $O_2$ and $H_2O_2$. With minor passivation layer coverage, their effect on the later adsorption has been revealed as shown in **Figure 6b**. Notably, the adsorption behaviours have apparently changed with the suppression of the O-O cleavage induced by over-reactivity of the surface. Within the preservation of the O-O bond, the bond length has slightly increased to 1.290 Å for $O_2$ and to 1.499 for $H_2O_2$, respectively. From the O-O bond length, the O-O dissociation will still happen on ortho-position configuration with the highest energy cost of 3.026 eV that might attribute to the facilitation from a strong interaction between two close oxygen atoms. From **Table 4** and **Figure 6c**, it is found that binding energies of $O_2$ and $H_2O_2$ have experienced an evident decrease on meta- and para-position oxygen passivation layer, which is in consistency with the surface adsorption behaviours. Thus, more stable oxygen molecules can be easier to bind near the surface. The binding energy of $H_2O_2$ on meta configuration is -0.464 eV, which will be the best site for desorption of formed $H_2O_2$ without over-binding. Another possible desorption site is above the para-position coverage configuration with binding energy around -1.267 eV. Even the Ru atoms on the surface are still active with the oxygen atom, both O-O bond in formed $H_2O_2$ has been maintained with $d_{O-O}$ at 1.481 Å and 1.499 Å. The strong electron transfer behaviours that are supposed to occur on the pristine surface will be relieved by the attached oxygen passivation layer on hollow sites, which prevents the over-interaction to cause decomposition or over-binding of $H_2O_2$. The passivation layer as the buffer layer become the dominant factor that can activate the surface from over-reactive to the proper catalyst, which can balance and optimize the surface adsorption reactions. Moreover, we notice that the oxygen coverage will rearrange to nearby hollow sites after relaxation, representing such passivation layer is relatively dynamic on the surface. Such preference might due to the repulsive force between oxygen atoms, which means that a low coverage might be able to achieve a high selectivity. **Figure**

**6d** further displays the $O_2$ adsorption energy with related to the different percentage of O-coverage (to quantitatively denote the oxidation state coverage rate), in forms of 0% (without coverage), 4.1% (very light coverage), and 12.5% (light coverage). A clear physicochemical down-trend can be noticed that to stabilize on the surface without any O-O bond cleavage, which indicates the passivation layer will promote the stabilities of $O_2$ on the surface of RuNi system. The influence of oxygen passivation layer to the dissociation of $H_2$ should also be taken into account, which will determine the productivity of $H_2O_2$. However, similar coverage models have proved that the cleavage of H-H bond will not be much affected with binding energy at 3.224 eV, which might be due to the much lower bond strength of H-H bond compared to O-O divalent bond.

Then we move our emphasis to the intermediates since the formation and stability of intermediates are also of importance for the investigation of the complete DSHP process, shown as follows. The relaxed structures of key species during DSHP are shown in **Figure 7a-7e**. The most important intermediates are OOH* that can directly lead to the formation of HOOH* as shown below.

$$O - O^* + H^* \rightarrow OOH^* \quad (8)$$

$$OOH^* + H^* \rightarrow HOOH^* \quad (9)$$

Hence, the formation energies of **Equation (8)** and **(9)** have been calculated as 1.05 eV and 0.57 eV, respectively. Especially, we have shown the initial positions of **Equation (8)** and **(9) in Figure 7g** and **7h,** in which the nearby free H* with 2.337 Å and 1.937 Å, respectively, will spontaneously migrate to O-O* and OOH* and form O-H bonds that result in the formation of OOH* and HOOH* species near the catalyst surface. Moreover, the dissociation of intermediate OOH* has also been effectively constrained on the oxygen passivated surface. The oxygen coverage configurations are highly related to the adsorption of the $O_2$, $H_2O_2$ and all the intermediate species, especially the

ortho-position coverage is the most unfavorable site for DSHP in both energy and selectivity. This can be ascribed to the much higher binding energy in comparison with the other two coverage configurations, accompanied by the undesired O-O cleavage.

Overall, the summarized reaction pathway in **Figure 7(f)** clearly exhibits a thermodynamically favorable DSHP process with a downhill energy trend along the reaction coordinates after self-activation through the oxygen coverage. At the initial stage of the adsorption process, the $H_2$ and $O_2$ will be attracted by the surface since the adsorption cost is much lowered with a close distance to the surface. The balance between the reactivity and stability are critical to the performance of the catalyst. With the passivation layer, the adsorption energies of $H_2$ remained similar meanwhile the oxygen adsorption has been affected evidently. The binding energy of $O_2$ has changed from positive to an appropriate negative level, suggesting a spontaneous reaction and a stable binding on the surface as expected. Thus, it can be expected that the free H* migration near the surface should be easy to achieve due to the smaller size of hydrogen atoms and much weaker bonding trend than the O* and $O_2$. In addition, the O-O dissociation is significantly suppressed on such covered surface that can improve the selectivity to $H_2O_2$ via decreasing the concentration of OH* intermediates. Compared to the dissociation of O-O bond, non-dissociation is much more energy favorable as shown in **Table 4**. Therefore, the reaction for formation of $H_2O_2$ has been changed from 2O*+2H* to O-O* + 2H* with energy cost decreased from 3.578 eV to 0.578 eV as shown in **Figure 7(f)**. At the final stage, the continued energy decrease from formed HOOH* to desorbed $H_2O_2$ as **Figure 7e** indicated a completely opposite trend with $H_2$ and $O_2$, which means the desorption of formed $H_2O_2$ is energetically favourable. In addition, the side product $H_2O$ displays extremely high energy cost on this RuNi (111) surface, which will be largely suppressed when competing with the DSHP process. Therefore, realizing DSHP with high selectivity on this catalyst

surface can be accomplished, in which the adsorption of $H_2$ is the rate determining step. The oxygen passivation layer determines the selectivity of $H_2O_2$ with suppression on the production of $H_2O$ during the proposed DSHP on the RuNi (111) surface.

With our calculation results, we can summarize a fundamental mechanism for the direct formation of $H_2O_2$ on the RuNi (111) (**Figure 8**). At the beginning stage of the DSHP on RuNi (111) surface, $O_2$ and $H_2$ will be compete with to each other on the adsorption to the surface and generate mobile O* and H*, in which $O_2$ has a slight advantage. Once the O-O bond has been cleaved, the O* will be quickly bonded on the hollow site and the formation of passivation film will start. The selectivity and productivity of $H_2O_2$ will be low at this initial stage since the formation of OH* intermediates induced by formed O*. After the initial stage, RuNi (111) will quickly be covered by oxygen passivation layer as the self-activation. Hence, the following adsorption of $O_2$ will be further lowered with preservation of the O-O bond, which will lead to enhancement of the selectivity and efficiency of forming $H_2O_2$. At this middle stage of catalysis, the adsorbed $O_2^*$ will attract the relatively free H* to form intermediate OOH* and even $H_2O_2$*. The generation of $H^*$ will continue without influence from oxygen passivation layer. With gradually formed $H_2O_2$* near the surface, the passivation layer can suppress the decomposition and the preferred de-adsorption of $H_2O_2$* at the certain active site on RuNi (111) surface can be realized consequently. The whole DSHP process will experience a slow production of $H_2O$ initially and a gradual increase of selectivity and productivity to $H_2O_2$ at the middle stage as the self-activation starts. As the coverage of the passivation layer has reached a certain level, the selectivity and productivity of $H_2O_2$ will become stable with the fully activated RuNi surface. In actual experiments, if the alloy can have partial oxidation through pre-treatment, the slow beginning stage in our proposed mechanism will

be much shortened and the efficiency of direct synthesis of $H_2O_2$ can be obviously increased based on direct activation.

**Conclusion**

In summary, we have predicted the RuNi (111) surface as a new Pd-free catalyst for DSHP based on the thorough investigation of the dynamic procedure of their self-activation mechanism. The over-activity of the RuNi surfaces or nanosphere particles can be ascribed to the activity of Ru in interacting with adsorbed molecules while Ni plays a role in balancing the activity to prevent excessive electron transfer and remaining the catalyst surface stability. The key factor affecting the selectivity and productivity is the self-activation process induced by partial passivation of the surface with oxygen coverage, which can significantly decrease the energy barrier for oxygen adsorption and suppress the O-O bond cleavage. The decomposition of formed $H_2O_2$ on the surface can also be successfully suppressed on most active sites under this condition. The self-activation has prevented the situation of the over-binding of $H_2O_2$ and lead to a reasonable desorption energy of formed $H_2O_2$. Therefore, RuNi can become the potential new catalyst for DSHP, which can open a new direction for future study in the catalyst area with better performance. The direct observation of the natural self-activation can assist in the comprehension of the dynamic catalytic process of active alloys.

**Figure 1.**

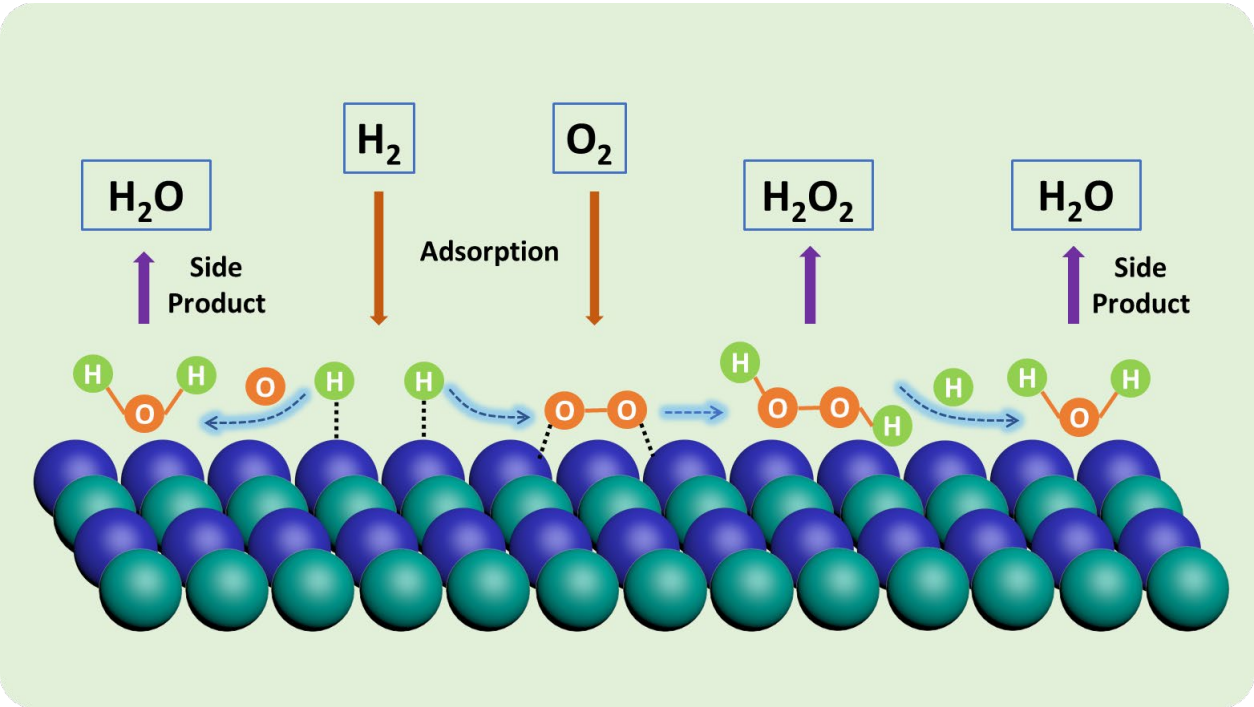


**Figure 1.** Mechanism of formation of $H_2O_2$ and side product $H_2O$ on the catalyst surface.

**Figure 2.**

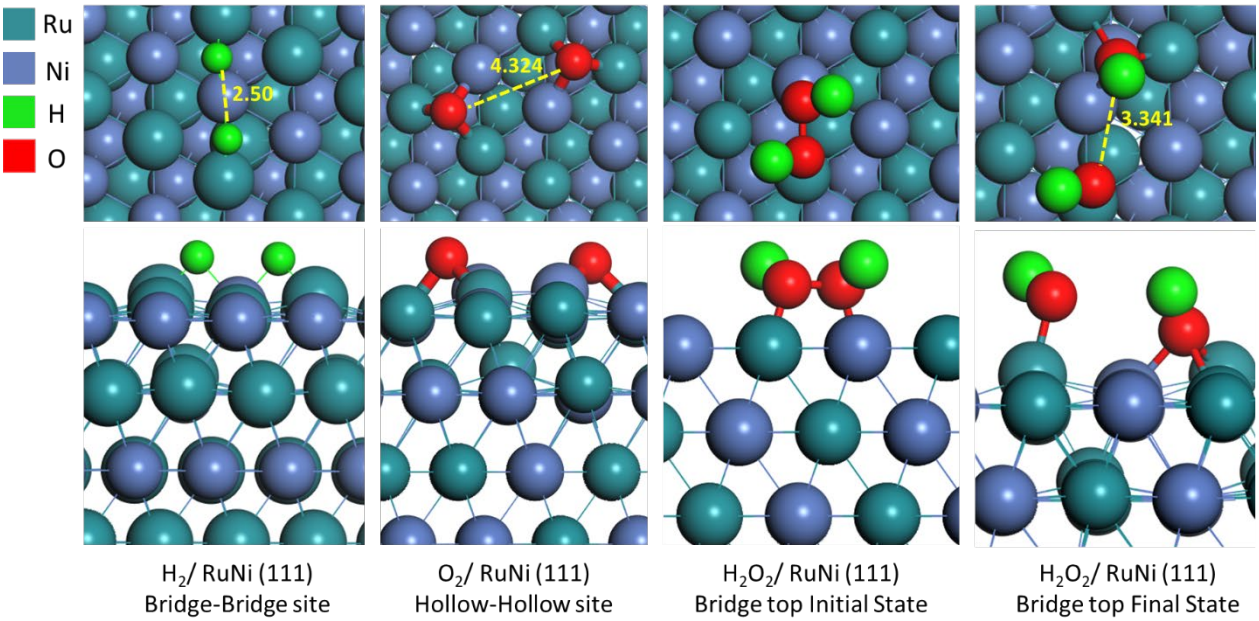


**Figure 2.** The top view and local view of most energy favourable site for adsorption of $H_2$, $O_2$, $H_2O_2$ on the pristine RuNi (111) surface after geometry relaxation.

**Figure 3.**

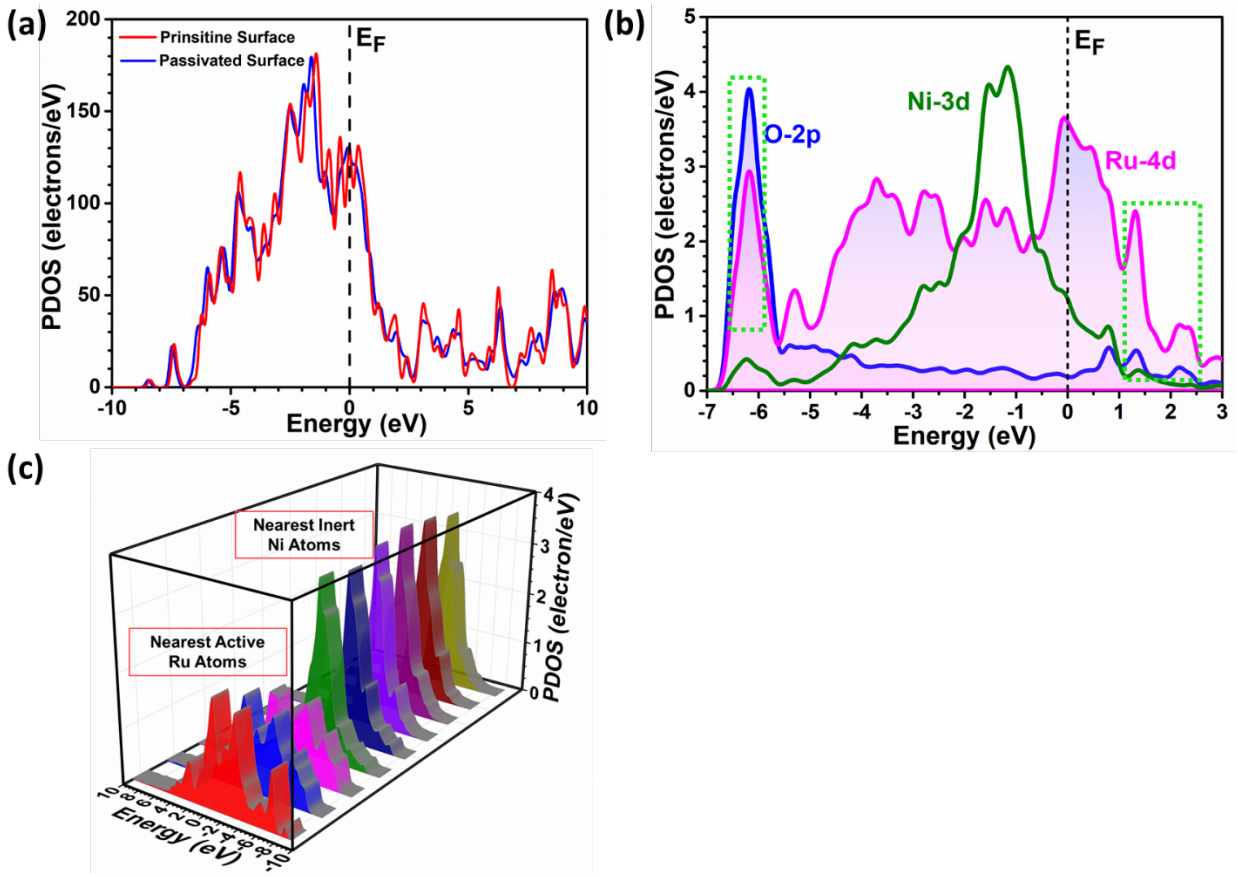


**Figure 3.** The Comparison of DOS between pristine and the oxygen partially covered RuNi surface. (a) Comparison of TDOS between the pristine surface and the passivated surface. (b) Illustration of the orbital overlap among O-2p orbitals, Ni-3d orbitals and Ru-4d orbitals. (c) The PDOS of d-orbitals of nearest Ru and Ni atoms of the passivation oxygen atoms.

**Figure 4.**

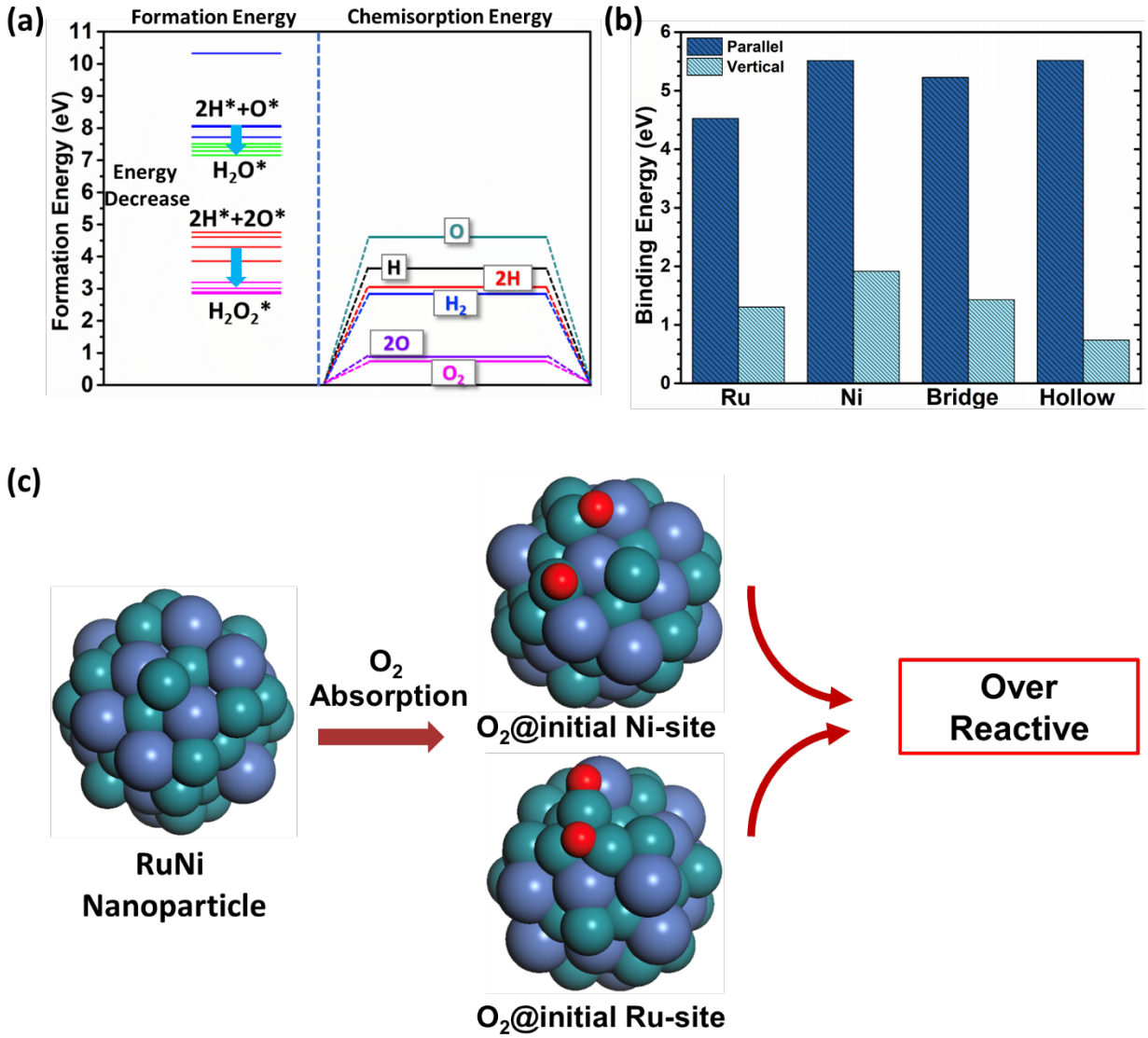


**Figure 4.** (a) **(Left)** Pure formation energies of $H_2O_2$ and $H_2O$. **(Right)** The chemisorption energy comparison of the RuNi (111) surface system. (b) Diagram of adsorption energies of adsorbed $O_2$ on RuNi surface at different sites (c) Illustration of over-reacting of RuNi nanoparticles with $O_2$.

**Figure 5.**

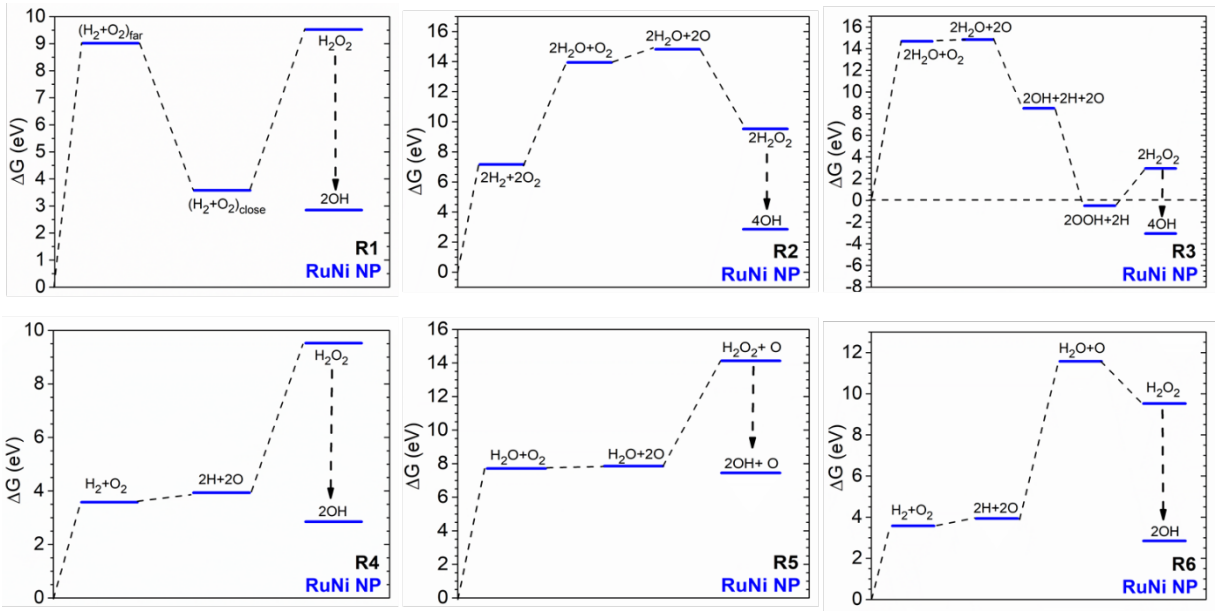


**Figure 5.** The energy profile of the proposed six possible reactions (R1 to R6) regarding the changes in free energy (ΔG) simulated on the Ru-rich surface of RuNi.

**Figure 6.**

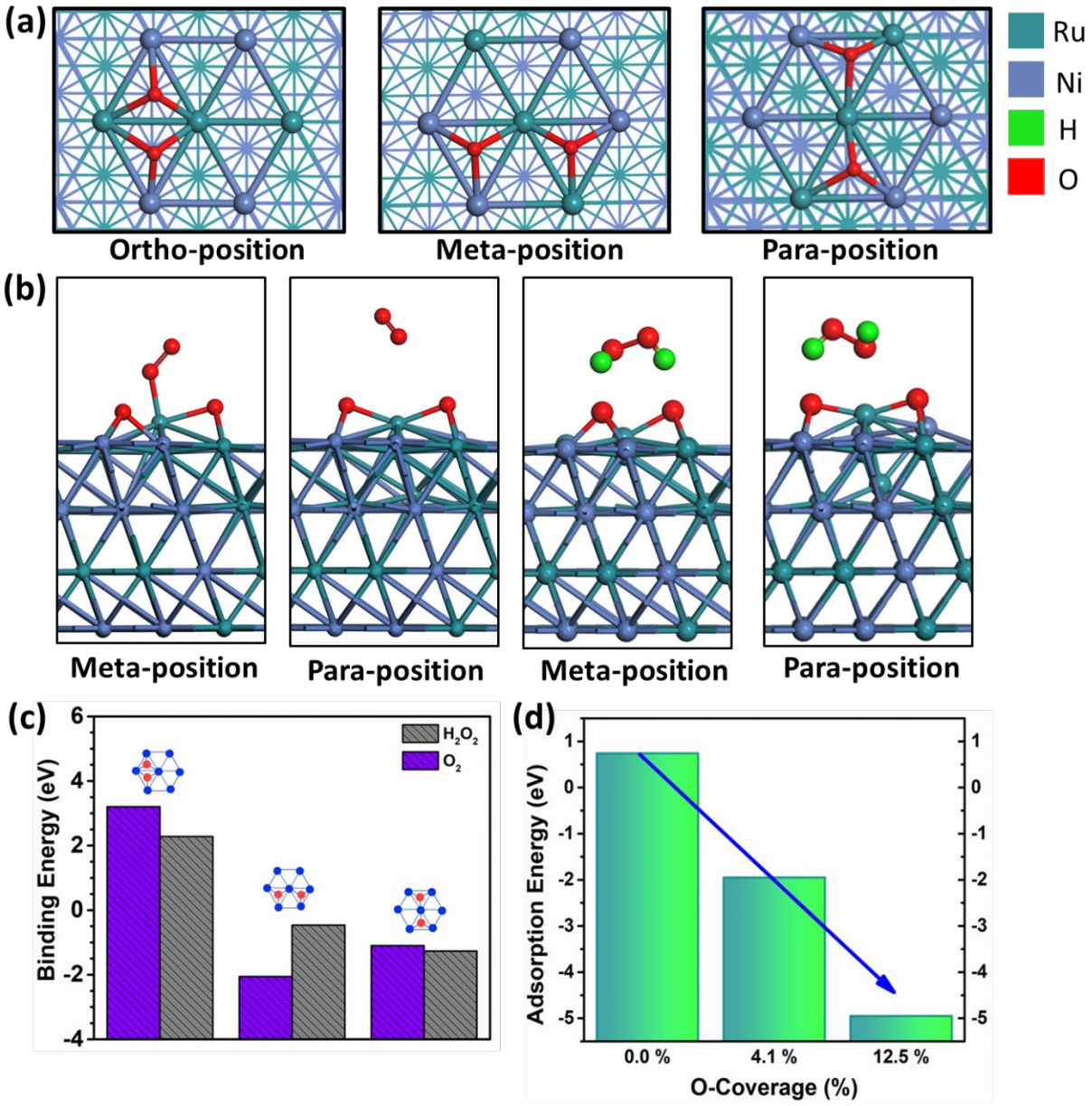


**Figure 6. The effect of oxygen passivation layer to the adsorption of $O_2$ and $H_2O_2$.** (a) Three oxygen coverage configurations as ortho-position, meta-position and para-position. (b) Local view of surface configuration after geometry relaxation of $O_2$ and $H_2O_2$ without O-O cleavage. (c) The binding energies of $O_2$ and $H_2O_2$ with the partially passivated RuNi surfaces. (d) The $O_2$ adsorption energy comparison with different O-coverage on the RuNi surface system.

**Figure 7.**

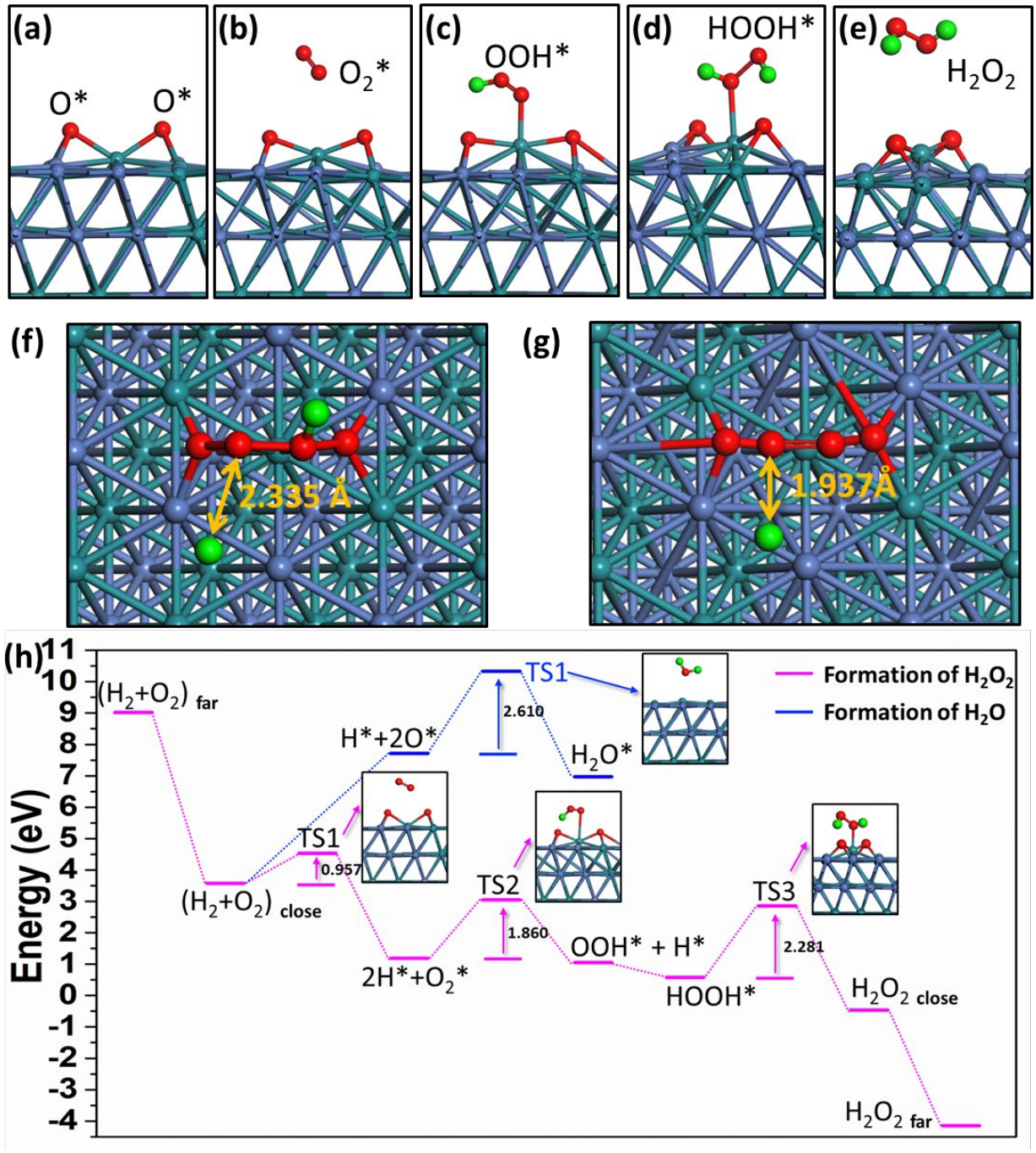


**Figure 7. Geometry structures of adsorption configuration and energy profile.** (a)-(e) Optimized structures of key steps in proposed DSHP on RuNi (111). (f)-(g) The initial

configuration of OOH* and HOOH*. (h)DFT calculated energy profile of the reaction coordinates on the RuNi (111) surface. The inset figures are the corresponding structure of transition states.

**Figure 8.**

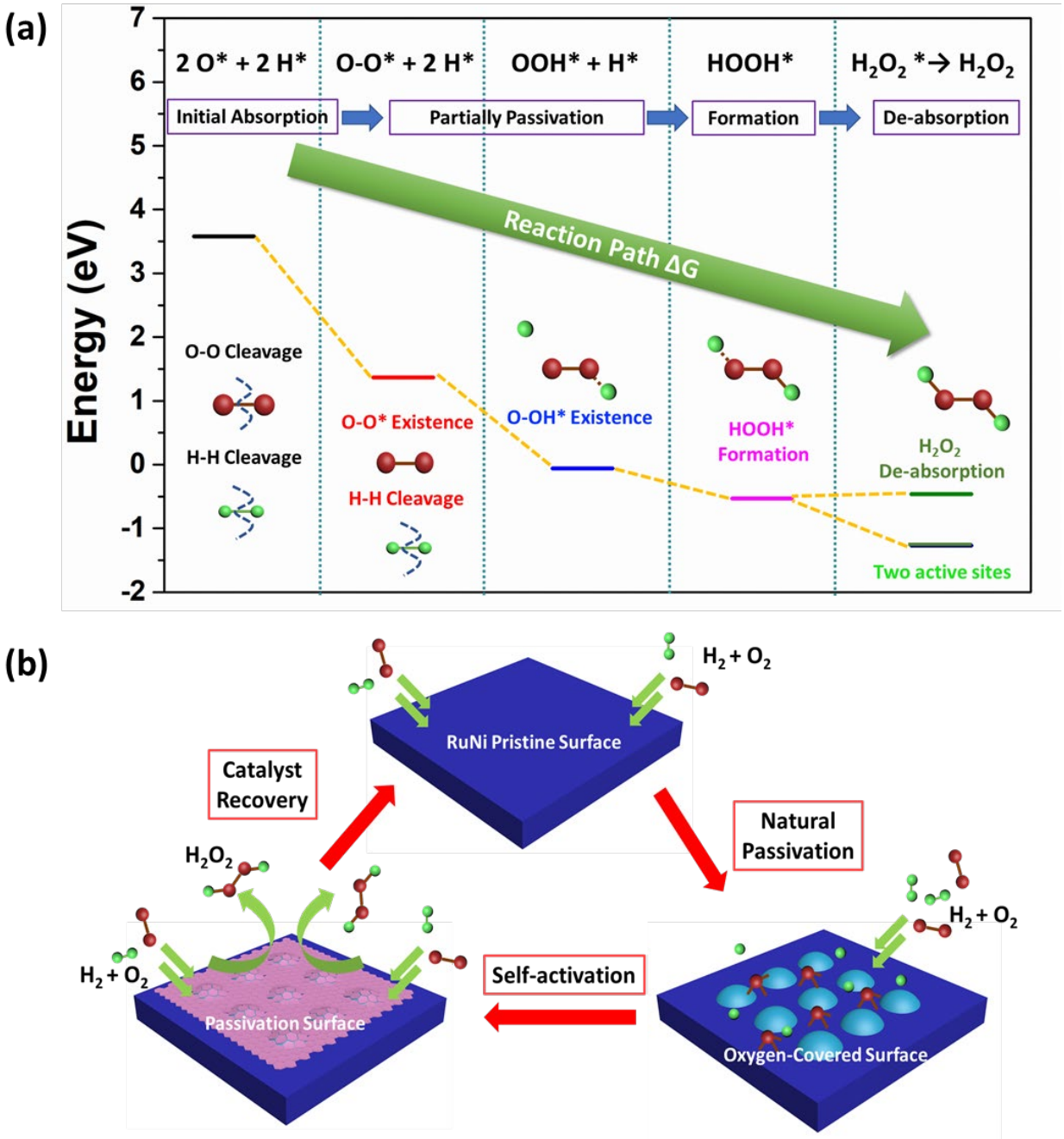


**Figure 8.** (a) The reaction path for direct synthesis of $H_2O_2$ on the RuNi (111) surface with the oxygen coverage assistance. (b) Illustration of DSHP process on the RuNi (111) surface.

**Table 1.** Adsorption Energies of $H_2$ and H atoms on the RuNi (111) surface

| Adsorption Site | $H_2$ Binding Energies (eV) | H atom Binding Energies (eV) | H atom Chemical Adsorption Energies (eV) |
|---|---|---|---|
| **Ru Top** | 2.993 | 3.827 | -0.597 |
| **Ni Top** | 2.839 | 3.796 | -0.571 |
| **Bridge Top** | 3.175 | 3.632 | -0.580 |
| **Hollow** | 3.115 | 3.868 | -0.755 |

**Table 2.** Adsorption Energies of $O_2$ and O atoms on the RuNi (111) surface

| Adsorption Site | $O_2$ Binding Energies (eV) | O atom Binding Energies (eV) | O atom Chemical Adsorption Energies (eV) |
|---|---|---|---|
| **Ru Top** | 1.305 | 5.041 | -3.283 |
| **Ni Top** | 1.918 | 7.490 | -6.306 |
| **Bridge Top** | 1.430 | 4.896 | -3.800 |
| **Hollow** | 0.739 | 4.604 | -3.723 |

**Table 3.** Adsorption Energies of $H_2O_2$ on the RuNi (111) surface

| Adsorption Site | $H_2O_2$ Binding Energies (eV) | $H_2O$ Binding Energies (eV) |
|---|---|---|
| **Ru Top** | 3.202 | 7.152 |
| **Ni Top** | 2.899 | 7.410 |
| **Bridge Top** | 2.846 | 7.286 |
| **Hollow Top** | 3.008 | 6.973 |

**Table 4.** Adsorption Energies of $H_2O_2$ on the oxygen passivated RuNi (111) surface

| Oxygen covered Site | $O_2$ Binding Energies (eV) | $d_{O\text{-}O}$ (Å) | $H_2O_2$ De-sorption Energies (eV) | $d_{O\text{-}O}$ (Å) |
|---|---|---|---|---|
| **Ortho-position** | 3.036 | 2.654 | 2.281 | 4.822 |

| | | | | |
|---|---|---|---|---|
| **Meta-position** | -2.055 | 1.290 | -0.464 | 1.499 |
| **Para-position** | -1.099 | 1.249 | -1.267 | 1.481 |

**Corresponding Author**

*Bolong Huang

E-mail: bhuang@polyu.edu.hk

**Author Contributions**

B.H conceived and led the project. B.H and M.S designed and operated the simulation modelling. B.H, M.S and X.L wrote the paper.

**Acknowledgment**

The author BH gratefully acknowledges the support of the Natural Science Foundation of China (NSFC) for the Youth Scientist grant (Grant No.: NSFC 11504309, NSFC 21771156), and the Early Career Scheme (ECS) fund (Grant No.: PolyU 253026/16P) from the Research Grant Council (RGC) in Hong Kong.

## References


1. P. B. Walsh, *Tappi J.*, 1991, **74**, 81-83.
2. J. M. Campos-Martin, G. Blanco-Brieva and J. L. Fierro, *Angew. Chem. Int. Ed. Engl.*, 2006, **45**, 6962-6984.
3. K. P. Bryliakov, *Chem. Rev.*, 2017, **117**, 11406-11459.
4. J. H. Teles, I. Hermans, G. Franz and R. A. Sheldon, 2015, 1-103.
5. A. Plauck, E. E. Stangland, J. A. Dumesic and M. Mavrikakis, *Proc Natl Acad Sci U S A*, 2016, **113**, E1973-1982.
6. S. J. Freakley, Q. He, J. H. Harrhy, L. Lu, D. A. Crole, D. J. Morgan, E. N. Ntainjua, J. K. Edwards, A. F. Carley, A. Y. Borisevich, C. J. Kiely and G. J. Hutchings, *Science*, 2016, **351**, 965-968.
7. J. K. Edwards, S. J. Freakley, R. J. Lewis, J. C. Pritchard and G. J. Hutchings, *Catal. Today*, 2015, **248**, 3-9.
8. Z. Zheng, Y. H. Ng, D. W. Wang and R. Amal, *Adv. Mater.*, 2016, **28**, 9949-9955.
9. T. P. Fellinger, F. Hasche, P. Strasser and M. Antonietti, *J. Am. Chem. Soc.*, 2012, **134**, 4072-4075.
10. P. A. Gravil, D. M. Bird and J. A. White, *Phys. Rev. Lett.*, 1996, **77**, 3933-3936.
11. N. M. Wilson and D. W. Flaherty, *J. Am. Chem. Soc.*, 2016, **138**, 574-586.
12. Q. Liu, J. C. Bauer, R. E. Schaak and J. H. Lunsford, *Angew. Chem.*, 2008, **120**, 6317-6320.
13. Q. Liu, J. C. Bauer, R. E. Schaak and J. H. Lunsford, *Applied Catalysis A: General*, 2008, **339**, 130-136.
14. E. N. Ntainjua, S. J. Freakley and G. J. Hutchings, *Top. Catal.*, 2012, **55**, 718-722.
15. A. Gervasini, P. Carniti, F. Desmedt and P. Miquel, *ACS Catalysis*, 2017, **7**, 4741-4752.
16. J. Zhang, B. Huang, Q. Shao and X. Huang, *ACS Appl Mater Interfaces*, 2018, DOI: 10.1021/acsami.8b03756.
17. M. Yan, Z. Q. Huang, Y. Zhang and C. R. Chang, *Phys. Chem. Chem. Phys.*, 2017, **19**, 2364-2371.
18. L. Ouyang, G.-j. Da, P.-f. Tian, T.-y. Chen, G.-d. Liang, J. Xu and Y.-F. Han, *J. Catal.*, 2014, **311**, 129-136.
19. Y. Nomura, T. Ishihara, Y. Hata, K. Kitawaki, K. Kaneko and H. Matsumoto, *ChemSusChem*, 2008, **1**, 619-621.
20. S. J. Freakley, Q. He, J. H. Harrhy, L. Lu, D. A. Crole, D. J. Morgan, E. N. Ntainjua, J. K. Edwards, A. F. Carley, A. Y. Borisevich, C. J. Kiely and G. J. Hutchings, *Science*, 2016, **351**, 965-968.
21. S. Maity and M. Eswaramoorthy, *Journal of Materials Chemistry A*, 2016, **4**, 3233-3237.
22. J. J. Van Veldhuizen, S. B. Garber, J. S. Kingsbury and A. H. Hoveyda, *J. Am. Chem. Soc.*, 2003, **125**, 12666-12666.
23. L. Zhang, X. Chen, P. Xue, H. H. Sun, I. D. Williams, K. B. Sharpless, V. V. Fokin and G. Jia, *J. Am. Chem. Soc.*, 2005, **127**, 15998-15999.
24. S. De, J. G. Zhang, R. Luque and N. Yan, *Energ Environ Sci*, 2016, **9**, 3314-3347.
25. S. Amendola, *Int. J. Hydrogen Energy*, 2000, **25**, 969-975.
26. A. Romero, A. Nieto-Márquez and E. Alonso, *Applied Catalysis A: General*, 2017, **529**, 49-59.
27. F. Liu, J. Y. Lee and W. J. Zhou, *Small*, 2006, **2**, 121-128.

28. E. Antolini, *Energies*, 2017, **10**, 42.
29. L. S. Ribeiro, J. J. Delgado, J. J. M. Órfão and M. F. R. Pereira, *Applied Catalysis B: Environmental*, 2017, **217**, 265-274.
30. H.-S. Roh, K.-W. Jun, W.-S. Dong, S.-E. Park and Y.-S. Baek, *Catal. Lett.*, 2001, **74**, 31-36.
31. L. Zhu, L. Zheng, K. Du, H. Fu, Y. Li, G. You and B. H. Chen, *RSC Adv.*, 2013, **3**, 713-719.
32. S. Tada, R. Kikuchi, K. Wada, K. Osada, K. Akiyama, S. Satokawa and Y. Kawashima, *J. Power Sources*, 2014, **264**, 59-66.
33. T. Deguchi and M. Iwamoto, *The Journal of Physical Chemistry C*, 2013, **117**, 18540-18548.
34. A. Verdaguer-Casadevall, D. Deiana, M. Karamad, S. Siahrostami, P. Malacrida, T. W. Hansen, J. Rossmeisl, I. Chorkendorff and I. E. Stephens, *Nano Lett.*, 2014, **14**, 1603-1608.
35. P. Tian, L. Ouyang, X. Xu, J. Xu and Y.-F. Han, *Chinese Journal of Catalysis*, 2013, **34**, 1002-1012.
36. S. J. Clark, M. D. Segall, C. J. Pickard, P. J. Hasnip, M. J. Probert, K. Refson and M. C. Payne, *Zeitschrift Fur Kristallographie*, 2005, **220**, 567-570.
37. J. P. Perdew, J. A. Chevary, S. H. Vosko, K. A. Jackson, M. R. Pederson, D. J. Singh and C. Fiolhais, *Physical Review B*, 1992, **46**, 6671-6687.
38. J. P. Perdew, K. Burke and M. Ernzerhof, *Phys. Rev. Lett.*, 1996, **77**, 3865-3868.
39. A. M. Rappe, K. M. Rabe, E. Kaxiras and J. D. Joannopoulos, *Physical Review B*, 1991, **44**, 13175-13176.
40. D. Dissanayake, *J. Catal.*, 2003, **214**, 113-120.
41. S. Chinta, *J. Catal.*, 2004, **225**, 249-255.
42. J. H. Lunsford, *J. Catal.*, 2003, **216**, 455-460.
43. S. Schwegmann, A. P. Seitsonen, V. De Renzi, H. Dietrich, H. Bludau, M. Gierer, H. Over, K. Jacobi, M. Scheffler and G. Ertl, *Physical Review B*, 1998, **57**, 15487-15495.
44. K.-W. Park, J.-H. Choi, B.-K. Kwon, S.-A. Lee, Y.-E. Sung, H.-Y. Ha, S.-A. Hong, H. Kim and A. Wieckowski, *The Journal of Physical Chemistry B*, 2002, **106**, 1869-1877.
45. K. Honkala and K. Laasonen, *The Journal of Chemical Physics*, 2001, **115**, 2297-2302.
46. J. Kim, X. Yin, K. C. Tsao, S. Fang and H. Yang, *J. Am. Chem. Soc.*, 2014, **136**, 14646-14649.
47. J. Suntivich, K. J. May, H. A. Gasteiger, J. B. Goodenough and Y. Shao-Horn, *Science*, 2011, **334**, 1383-1385.
48. Y. Tong, Y. Guo, P. Chen, H. Liu, M. Zhang, L. Zhang, W. Yan, W. Chu, C. Wu and Y. Xie, *Chem*, 2017, **3**, 812-821.
49. R. Todorovic and R. J. Meyer, *Catal. Today*, 2011, **160**, 242-248.
50. D. Gudarzi, W. Ratchananusorn, I. Turunen, M. Heinonen and T. salmi, *Catal. Today*, 2015, **248**, 69-79.

**ToC Figure**

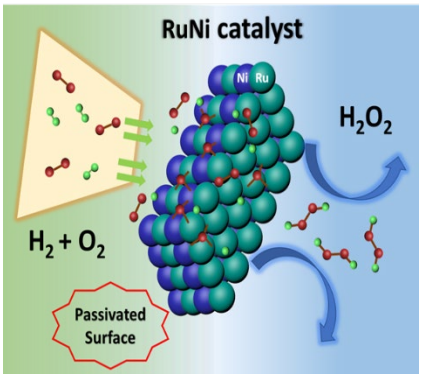


**Illustration of RuNi as the efficient catalyst for DSHP**